Quantitative Rietveld texture analysis of $CaSiO_3$ perovskite deformed in a diamond anvil cell

2006 J. Phys.: Condens. Matter 18 S995

(http://iopscience.iop.org/0953-8984/18/25/S07)

INSTITUTE OF PHYSICS PUBLISHING JOURNAL OF PHYSICS: CONDENSED MATTER

J. Phys.: Condens. Matter **18** (2006) S995–S1005 doi:10.1088/0953-8984/18/25/S07

Quantitative Rietveld texture analysis of $CaSiO_3$ perovskite deformed in a diamond anvil cell

Lowell Miyagi[1], Sébastien Merkel[1], Takehiko Yagi[2], Nagayoshi Sata[3], Yasuo Ohishi[4] and Hans-Rudolf Wenk[1]

[1] Department of Earth and Planetary Science, University of California, Berkeley, CA 94720, USA
[2] Institute for Solid State Physics, University of Tokyo, Kashiwanoha 5-1-5, Kashiwa, Chiba 277-8581, Japan
[3] Institute for Research on Earth Evolution, Japan Agency for Marine-Earth Science and Technology, Natsushima-cho, Yokosuka, Kanagawa 237-0061, Japan
[4] Japan Synchrotron Radiation Research Institute, Mikazuki-cho, Sayo-gun, Hyogo 679-5198, Japan

Received 30 November 2005, in final form 25 April 2006
Published 8 June 2006
Online at stacks.iop.org/JPhysCM/18/S995

Abstract

The Rietveld method is used to extract quantitative texture information from a single synchrotron diffraction image of a $CaSiO_3$ perovskite sample deformed in axial compression in a diamond anvil cell. The image used for analysis was taken in radial geometry at 49 GPa and room temperature. We obtain a preferred orientation of {100} lattice planes oriented perpendicular to the compression direction and this is compatible with $\{110\}\langle 1\bar{1}0\rangle$ slip.

1. Introduction

Although $CaSiO_3$ perovskite is thought to be the major calcium silicate component of the lower mantle, its properties are still poorly understood. Even the structure that $CaSiO_3$ assumes at high pressures is not well defined. Experimentally, $CaSiO_3$ perovskite is generally reported to assume a cubic structure [1, 2]. Shim *et al* [3] reported a lower symmetry structure based on high resolution synchrotron data, and proposed several possible tetragonal structures. Theoretical calculations have predicted small symmetry lowering distortions of the cubic structure which yield tetragonal or even orthorhombic symmetries [4, 5]. Caracas *et al* [6] predict a multitude of structural instabilities with minor distortions of the cubic lattice that would be barely discernable in x-ray data. These symmetry lowering distortions are accomplished by rotation or distortion of the $Si–O_6$ octahedra.

The deformation mechanisms of $CaSiO_3$ perovskite are also poorly understood, and this is largely due to the fact that it is unquenchable to ambient conditions. This is a problem commonly encountered in the study of mineral phases that compose the deep earth. One way that mechanical properties at high pressures have been studied is through the use of diamond anvil cells (DACs) in radial diffraction geometry [7, 8]. Radial diffraction yields information on lattice strains as well as lattice preferred orientation (texture).

In synchrotron diffraction images, preferred orientation manifests itself as systematic intensity variations along Debye rings. If the lattice planes in a sample are predominantly oriented in a particular direction, more intense diffraction will be observed in the corresponding position on the Debye ring. It has been shown that the full orientation distribution (OD) can often be determined from a single two-dimensional synchrotron diffraction image utilizing the Rietveld method [9]. Here we perform quantitative texture analysis on radial diffraction measurements taken *in situ* on $CaSiO_3$ perovskite deformed in a DAC at high pressure. The emphasis is on the procedure of the refinement.

2. Experimental technique

Starting material of $CaSiO_3$ wollastonite, ground to a fine powder and mixed with amorphous boron to serve as laser absorber, was loaded into an 80 μm hole in an amorphous boron–epoxy gasket supported by a kapton confining ring [10]. The starting thickness of the amorphous boron–epoxy insert was 40 μm with an outer diameter of 400 μm. The sample was compressed with 350 μm diameter culet flat diamonds in a laser heated diamond anvil cell with large openings to allow radial diffraction. The starting material was initially compressed to a pressure of about 20 GPa. At this pressure, the phase transformation to the perovskite phase was induced by heating with a focused yttrium–aluminium–garnet laser on one side. The pressure was then increased in steps up to 49 GPa. Angle-dispersive x-ray diffraction spectra were collected in radial geometry with a 2000 $\times$ 2000 pixels Rigaku imaging plate at beamline BL10XU of SPring-8 using a monochromatic incident x-ray beam (wavelength 0.412 Å) of 20 μm in diameter. The exposure time was of the order of 15 min. The sample to detector distance (447.6 mm) and detector tilt were calibrated with a CeO_2 standard taken prior to the experiment. In order to accommodate a shift in the position of the imaging plates between each exposure, the direct beam was exposed briefly at the beginning of each exposure and used for beam centre calibration at each pressure. The image used in the present study is shown in figure 1.

3. Data processing

The MAUD (material analysis using diffraction) software package [11] was used to perform texture analysis via the Rietveld method. Prior to analysis, the images were first processed in FIT2D [12]. The beam centre was found using the 2D Gaussian fit function. Distortions due to tilt, as well as sample to detector distance, were calibrated with the CeO_2 standard. The cake function was used to select the start and end azimuth and 2θ range. A macro was then used to prepare a series of chi files of integrated slices. For this analysis the full 360° coverage was integrated over 5° increments of the azimuth angle into 72 slices and saved in 2θ versus intensity text files. The text files were converted into an esg format file and imported into the data files window in MAUD as spectra for refinement. Images in tiff format can also be processed directly in MAUD using the image manager function. In this case it is necessary to designate the beam centre, azimuth range, increment of integration, and outer limit for integration. Once integration is complete an esg file (input file for MAUD) is produced. Rietveld refinement proceeded as follows.

(1) First esg files for the CeO_2 standard were imported. Instrument geometry, measurement type, source, and detector type were selected under instrument options. Wavelength and detector distance were also entered. Spectra from the CeO_2 standard were used to calibrate Caglioti and Gaussian peak profile parameters. Background parameters and crystallite size

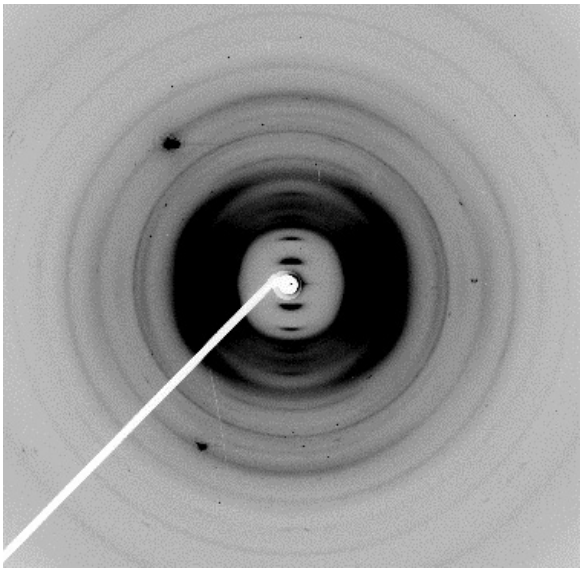

Figure 1. Diffraction pattern of $CaSiO_3$ at 49 GPa. The small spot in the centre of the beam stop is the mark from briefly exposing the direct beam. The gasket assembly diffracts at low 2θ angles producing the dark region in the middle of the image. Note also the presence of the beam stop arm and diamond spots.

were refined along with the Caglioti and Gaussian values. Once calibration was finished, Caglioti and Gaussian peak profile parameters were fixed and CeO_2 spectra were removed.

(2) The diffraction pattern of $CaSiO_3$ perovskite (figure 1) was processed and imported. Spectra containing diamond spots or the beam stop arm were removed from the refinement, and a 2θ range was designated.

(3) A structure model for $CaSiO_3$ perovskite was selected from a mineral database. In this case a cif (crystallographic information file) with space group $Pm\bar{3}m$ was used [13]. Models can also be built manually in MAUD by designating the space group, chemical composition, atomic positions, temperature factors, and oxidation states.

(4) Backgrounds were fitted to a seventh-order polynomial in a plotting program and these values were used in MAUD to define global background parameters. Global backgrounds were fixed and third-order polynomial backgrounds were added to each of the spectra to account for variations with azimuth. Individual backgrounds were refined along with incident intensity and lattice parameters to adjust the peak height and position.

(5) A strain model was then selected for the sample. Moment pole stress [14] with the Reuss model was used. For cubic symmetry only C_{11}, C_{12}, and C_{44} are needed to define the full elastic tensor. All other C_{ij} values were fixed accordingly ($C_{11} = C_{22} = C_{33}$, $C_{12} = C_{13} = C_{23}$, and $C_{44} = C_{55} = C_{66}$). According to the geometry of stress in diamond anvil cell radial diffraction experiments, macrostresses were fixed with $\sigma_{ij} = 0$ for $i \neq j$, $\sigma_{11} = \sigma_{22}$, and $\sigma_{33} = -2\sigma_{11}$, where σ_{33} is the largest principal stress. With the conventions implemented in MAUD, σ_{33} is negative for compression. With these constraints imposed, σ_{11} was freed and the parameters were refined. In the initial refinement of the stress model, the pressure was estimated and C_{ij}s were calculated for the pressure based on the theoretical values of Karki and Crain [4]. Once the lattice parameters converged, the pressure was calculated using the third-order Birch–Murnaghan equation of

state and values of K_{T0} and K'_{T0} from Shim *et al* [15, 16]. The elastic constants were then recalculated at this pressure and entered into the strain model.

(6) To fit peak heights and shapes, isotropic crystallite size and microstrains were refined with all the previous parameters. To determine the crystallite size, Popa line broadening [17] with an isotropic size-strain model was used.

(7) Isotropic thermal vibrations were then freed for each of the atoms to improve the balance of the relative intensities of peaks with respect to each other. This parameter is the isotropic B-factor, which is given by $B = 8\pi^2\langle u\rangle^2$, where $\langle u\rangle^2$ is the mean-squared amplitude of vibration [18]. Care should be taken to ensure that none of the B-factors become negative.

(8) Once a reasonably good fit ($R = 2.22$ and $R_w = 2.87$) was attained, a texture model was selected for calculation of the orientation distribution function (ODF). The R-factor in MAUD is equivalent to the 'R-structure factor' or R_F and R_w is analogous to the 'R-weighted pattern' or R_{wp} [19]. The difference between the R_w of MAUD and R_{wp} is that R_w is taken over all the patterns used in the texture analysis rather than over just the one pattern that would be used for a standard Rietveld analysis.

(9) Quality of a fit is conveniently shown in a map plot, analogous to a 'cake' in Fit 2D. The experimental data set is shown in figure 2(a). A map plot of the fit prior to texture refinement is shown in figure 2(b). The tomography based E-WIMV algorithm which is similar to WIMV [20] was used for the texture refinement. An ODF grid size of 10° and tube projection radius of 20° were used. Initially no symmetry was imposed and the texture was refined with the other parameters. An R-value of 1.97% and an R_w of 2.45% were obtained. A map plot of the refinement without symmetry imposed is shown in figure 2(c), and selected profiles are shown in figures 3(a) and (b).

(10) Pole figures of (100), (110), and (111) poles were calculated from the ODF (figure 4(a)). Pole densities are expressed in multiples of a random distribution (mrd). The textures are approximately axially symmetric about the compression axis (centre).

(11) Once it was verified that the textures were approximately symmetric, the ODF was reset and cylindrical symmetry was imposed. A map plot is shown in figure 2(d). With a symmetric texture R and R_w increased slightly to 2.09% and 2.65% respectively. This is due to the fact that textures in a DAC are not perfectly axially symmetric. The change in the quality of fit can be seen particularly well in the (210) peak (figures 2(c), (d)). Along this peak, intensity variations fit well in the instance where no symmetry was imposed. However, once cylindrical symmetry is imposed intensity variations along this peak are not as well correlated between the calculated and experimental data. One can also see that intensity maxima along other peaks are more symmetric than in the initial refinement. These differences are very slight, reconfirming that the assumption of cylindrical symmetry is justified. Other aspects of the fit have remained the same. Pole figures with symmetry imposed (figure 4(b)) are similar to those previously plotted but have a slightly lower maximum. This is a result of the averaging of the ODF to meet symmetry requirements. From the ODF with symmetry imposed an inverse pole figure of the compression direction was calculated.

4. Results

Crystallographic and microstructural parameters from the refinement and values for elastic constants are shown in table 1. Errors are indicated in parentheses. It should be noted that in general errors calculated by Rietveld refinement tend to be underestimated [21]. Estimated

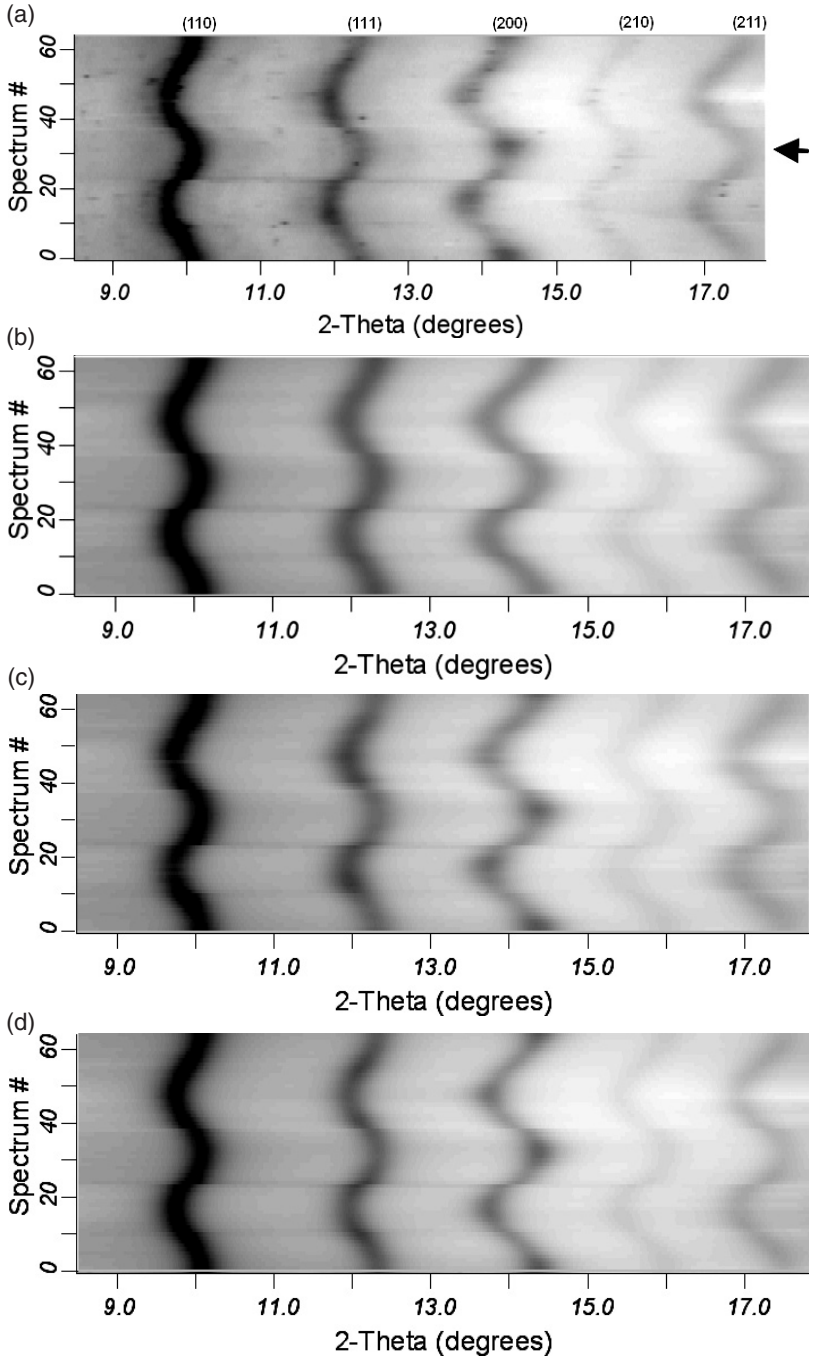

Figure 2. (a) Map plot of the experimental data with the compression direction indicated by an arrow. Peaks are labelled for reference. (b) Fit to the data prior to refinement of texture. Backgrounds are well correlated as are sinusoidal variations due to non-hydrostatic stresses. Intensity variations (texture) are still not matched. ((c) and (d)) Map plots showing the quality of fits after texture refinement for (c) no symmetry imposed, (d) cylindrical symmetry imposed. In (c), texture with no symmetry shows a good fit of the intensity variations. With symmetry imposed in (d), the quality of the fit is slightly lower. In the (111) peak (second peak from the left) the intensity maxima do not correlate as well as in (c).

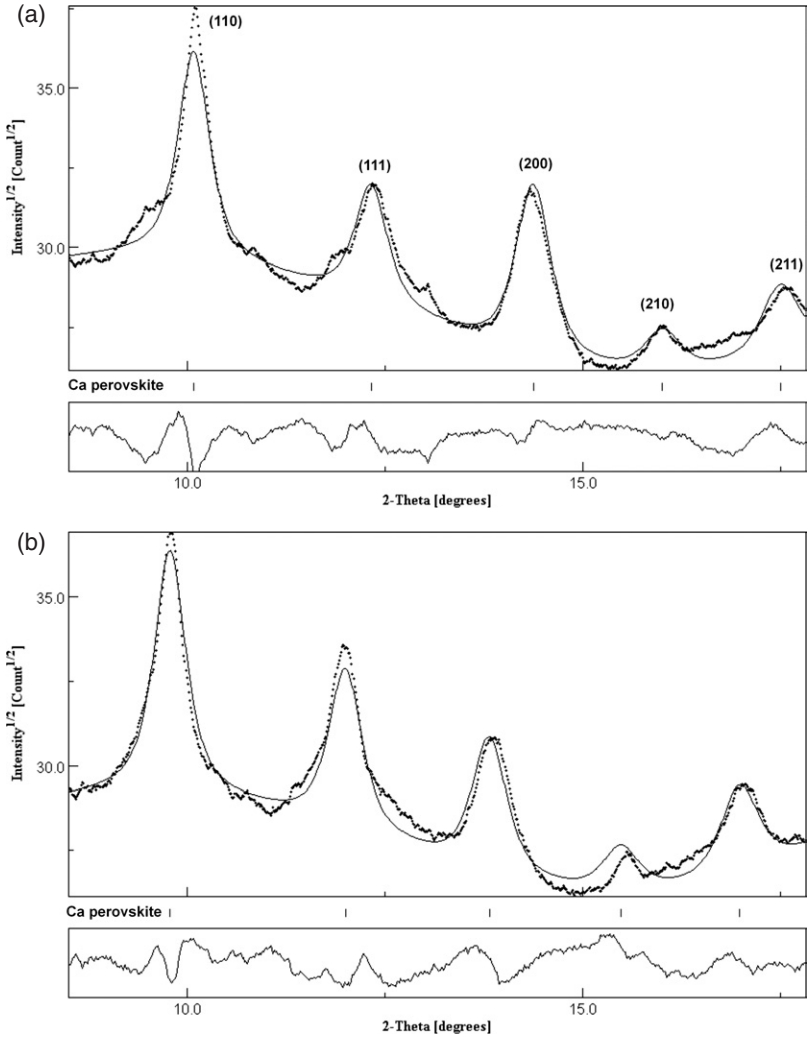

Figure 3. Diffraction profiles along (a) compression direction and (b) extension direction. For the profiles shown in (a) and (b), slight mismatches in the 2θ variation can be seen in these two orientations. Texture is visible as an intensity variation between corresponding peaks at these two different azimuths. Difference plots are shown below (a) and (b).

standard deviations are only a measure of the precision and do not account for additional errors introduced during the experiment or calibration.

Texture results for an ODF which is axially symmetric are conveniently represented by the inverse pole figure of the compression direction. The inverse pole figure is shown in figure 5. In this case only the cubic sector is needed to represent the texture. It shows a ⟨100⟩ maximum with a shoulder towards ⟨110⟩ and a depleted region around ⟨111⟩. The textures are moderate, with a maximum of 1.5 times random distribution.

5. Considerations on Rietveld refinement

Diffraction patterns of samples in DAC often contain large diamond spots. Since these are the result of single crystal diffraction, in many cases it is possible to rotate the DAC a few

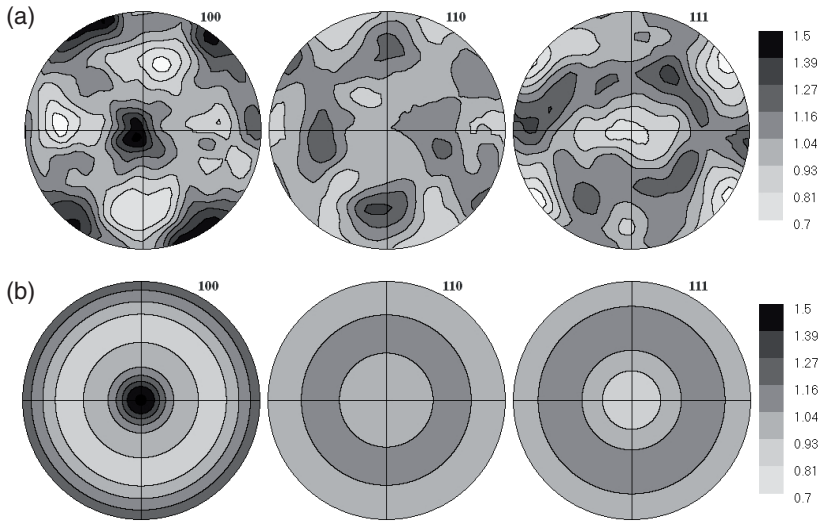

Figure 4. Pole figures plotted for (a) no symmetry imposed and (b) cylindrical symmetry imposed. The centre of the figures corresponds to the compression direction. Pole figures are equal area projections with linear contours (in mrd). In the case of (a) it can be seen that the textures are approximately axially symmetric. The pole figures in (b) are averaged to meet the requirements of the imposed symmetry. This results in the slightly lower maximum observed in (b). Both sets show a distinct maximum of ⟨100⟩ in the compression direction.

Table 1. Refinement parameters from MAUD. Errors are shown in parentheses. Incident intensity and microstrain are unitless. Values of the elastic constants are for a pressure of 49 GPa.

Refinement parameters from MAUD	
Parameter	Value (error)
Incident intensity	1.589 (0.007)
Lattice parameter a (Å)	3.3959 (0.0001)
Crystallite size (Å)	43.00 (0.1)
Microstrain	0.0048 (0.0001)
σ_{33} (Gpa)	−12.56(0.03)
Ca isotropic B-factor (Å^2)	2.017 (0.04)
Si isotropic B-factor (Å^2)	12.62 (0.05)
O isotropic B-factor (Å^2)	7.50 (0.03)
C_{11} (GPa)	712.4 (fixed)
C_{12} (GPa)	291.9 (fixed)
C_{44} (GPa)	310.5 (fixed)

degrees, avoiding diffraction conditions and thereby removing the spots. However, it is not always possible or convenient to take these precautions. Absorption from the beam stop arm can also hamper refinement. To remedy this, of all 72 spectra, seven spectra, one containing the beam stop arm and six containing large diamond spots, were discarded from the refinement.

Radial diffraction geometry introduces the additional complication that the x-ray beam not only passes through the sample but also through the gasket and the diamonds. An advantage of the boron and kapton gasket assembly is that diffraction from the gasket is almost entirely due to the kapton and only occurs at low angles [10]. Likewise, absorption effects from the

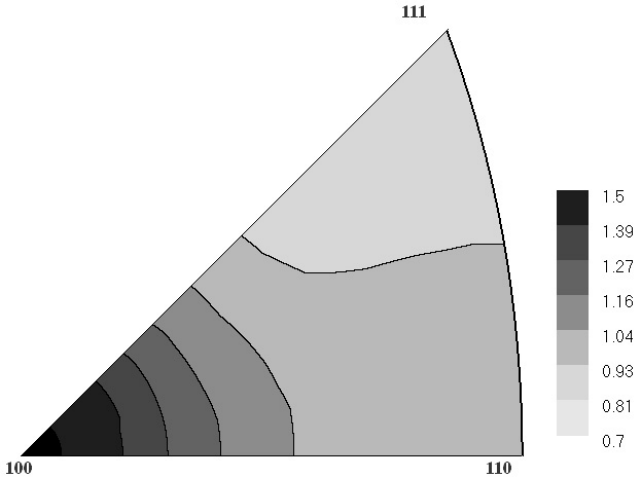

Figure 5. Equal area projection of the inverse pole figure for the compression direction. The scale is in multiples of random distribution (mrd).

diamonds are most problematic at low angles (figure 1). In order to avoid this region, the refinement was restricted to the 2θ range 8.5°–18.1°.

Because of probable stress gradients and weak diffraction from $CaSiO_3$, peaks are of low intensity and quite diffuse. One complication resulting from this is that backgrounds are difficult to fit. This was remedied by plotting one spectrum with a representative background in an independent plotting program, manually selecting points along the background, and fitting them with a seventh-order polynomial. This was then used to assign values for global background parameters in MAUD. In this case, this method proved considerably faster than fitting backgrounds directly in MAUD. Poorly resolved peaks can also make proper assignment of a crystal structure difficult as it may be impossible to observe subtle peak splits. This is particularly a problem in this analysis since several non-cubic structures, resulting from minute distortions of the cubic structure, have been proposed for $CaSiO_3$ [4–6].

Refinement with the cubic $Pm\bar{3}m$ structure did not properly account for the relative intensities of the peaks. In order to address this issue, we investigated the effects of several non-cubic structures on the refinement. The structures used were $P4/mmm$, $I4/mcm$, $Pnma$, and $Pbnm$. For all cases it became clear by visual inspection that the cubic structure provided the best match to the data. Consequently the $Pm\bar{3}m$ structure was retained and used for refinement. To obtain a better fit, isotropic thermal parameters were refined.

Complications in calculating the texture may occur if the stress model does not accurately predict the variation of d-spacing with azimuth that results from lattice strains. If the model is not correct the variation with azimuth may be overestimated for some peaks and underestimated for others. If the peak positions are not matched, the intensities will be fitted based on where the calculated peak intersects the data and this may not be the maximum intensity. If this is the case, intensity variations along a given Debye ring will not be accurately modelled and errors in the texture extraction may result. Although the stress model used in this refinement provides a reasonably good fit for these variations in lattice spacing, there are some slight mismatches in peak positions and intensities between the calculated model and the experimental data. For example, in figures 3(a) and (b), the (210) peak is well correlated in figure 3(a) but is shifted to the left in figure 3(b), resulting in an artificially high intensity maximum for that orientation. It

is likely that this is due to a few degrees of deviation in the maximum compression axis from the diamond axis [22].

One way to resolve this issue is to refine the elastic constants. We chose to refine the shear related elastic constants C_{12} and C_{44}, as variations in d-spacing should be more sensitive to these than to C_{11} [23, 24]. These constants were refined in two separate refinements, the first resulting in a 20% decrease for C_{12} and the second a 12% decrease in C_{44}. No significant difference in the quality of fit between these two refinements could be observed. As is often the case for cubic minerals, the texture is not very sensitive to these minor mismatches in the stress model and the texture results from these two refinements were practically identical to the initial texture calculation.

6. Discussion

The lattice parameter obtained from the refinement correlates well with values from previous experimental work as well as theoretical values for corresponding conditions [3–5, 15, 16, 25]. It is likely, however, that there are additional errors associated with this parameter. For example, the sample may have moved slightly during the experiment as a result of removing the DAC to increase the pressure. As a consequence the actual error for this parameter is probably much higher than the given value.

The crystallite size is unreasonably small. This could be partially due to imperfect calibration of the Caglioti function from the standard. Since the crystallite size is determined from the peak shapes, if aberrations in peak broadening are not properly corrected, the crystallite size obtained will have larger errors. In addition the peaks are not well resolved from the background and appear broader. This may result in obtaining an artificially low crystallite size that correlates with peak broadening. It is important to note that crystallite size is not synonymous with grain size, but refers to the size of the coherently scattering domains within the grains.

For a well defined crystal structure, isotropic B-factors should be positive and less than 1 $Å^2$; however, they are significantly higher. This most likely indicates that the structure model is not entirely correct. If $CaSiO_3$ perovskite in the sample is not truly cubic but pseudo-cubic, deviations from the cubic structure would cause the calculated thermal parameters to be large for those atoms which are misplaced in the model. The especially large thermal vibrations associated with Si and O atoms could support some sort of rotation or distortion of the Si–O_6 octahedra. It is also possible that a variety of these structures could exist in the sample.

We obtain a value of -12.6 GPa for σ_{33}. In the convention used in MAUD the negative value indicates a compressive stress. This corresponds to an axial stress component t of 18.9 at 49 GPa. This is considerably higher than the value found by Shieh *et al* [25], who found that the axial stress component increased from 3 GPa at a pressure of 19 GPa to 11 GPa at 61 GPa for $CaSiO_3$ perovskite. Our value is also larger than deviatoric stresses previously obtained in DAC experiments [8]. The actual stress depends on many factors, including the gasket material.

Based on geometrical considerations as well as TEM observations on a variety of perovskites ($KNbO_3$, $KTaO_3$, $BaTiO_3$, $CaTiO_3$, and $MnGeO_3$), Poirier *et al* [26] proposed that crystals with the cubic perovskite structure deform on the $\{110\}\langle 1\bar{1}0\rangle$ slip system at room temperature and on both the $\{110\}\langle 1\bar{1}0\rangle$ and $\{100\}\langle 001\rangle$ systems at high temperatures. These slip systems have also been observed in $SrTiO_3$ perovskite [27] and in $CaTiO_3$ [28]. No texture information is available on these materials except for a simple shear experiment on $CaTiO_3$ [29]. The proposed slip systems for cubic perovskite are similar to those of the cubic mineral halite [30, 31] and periclase [8]. In this case texture information is available and can be compared with our new results for $CaSiO_3$ perovskite.

In halite and periclase at low temperature, deformation in compression produces a ⟨100⟩ maximum parallel to the compression direction. Self-consistent polycrystal plasticity modelling of the compression of halite with hardening and dominant {110}⟨1$\bar{1}$0⟩ slip produces inverse pole figures that are strikingly similar to the inverse pole figure obtained for $CaSiO_3$ perovskite [32]. This family is particularly interesting because the two slip systems (110) ⟨1$\bar{1}$0⟩ and (1$\bar{1}$0) ⟨110⟩ are equally favoured and their resulting plastic rotations cancel. Texture in this case develops as a result of flattening of grains and shape-dependent rotation [33]. Based on these considerations, we conclude that the $CaSiO_3$ texture is compatible with {110}⟨1$\bar{1}$0⟩ slip as has been identified for cubic perovskite at low temperatures [26–28].

7. Conclusions

Quantitative texture analysis by the Rietveld method as implemented in MAUD is used to gain insight into the deformation mechanisms of $CaSiO_3$ perovskite at high pressures and room temperature. Using a single synchrotron image taken in radial geometry at 49 GPa we obtain a compression texture with {100} lattice planes oriented perpendicular to the compression. This indicates that (110) ⟨1$\bar{1}$0⟩ slip is the dominant slip system. The refinement suggests that deviatoric compressive stresses in the DAC were 18.9 GPa at 49 GPa. The crystallographic and microstructural parameters are consistent with a distortion of the cubic structure. This paper illustrates a relatively quick and convenient method to obtain quantitative texture and structure information from materials deformed at high pressure conditions.

Acknowledgments

The synchrotron radiation experiments were performed at the BL10XU in SPring-8 with the approval of the Japan Synchrotron Radiation Research Institute (JASRI) (Proposal No. 2003B0243-ND2b-np). The authors would like to thank I Lonardelli, S Speziale, and M Kunz for their valuable discussions, H Liu and COMPRES for an exciting workshop at APS, and two anonymous reviewers whose comments improved the manuscript. L Miyagi greatly appreciates support given by CDAC.

References

[1] Mao H-K, Chen L C, Hemley R J, Jephcoat A P, Wu Y and Bassett W A 1989 *J. Geophys. Res.* **94** 17889–94
[2] Wang Y, Weidner D J and Guyot F 1996 *J. Geophys. Res.* **101** 661–72
[3] Shim S H, Jeanloz R and Duffy T S 2002 *Geophys. Res. Lett.* **29** 2166 doi:10.1029/2002GL016148
[4] Karki B B and Crain J 1998 *Geophys. Res. Lett.* **25** 2741–4
[5] Akber-Knutson S, Bukowinski M S T and Matas J 2002 *Geophys. Res. Lett.* **29** 1034 doi:10.1029/2001GL013523
[6] Caracas R, Wentzcovitch R, Price G D and Brodholt J 2005 *Geophys. Res. Lett.* **32** L06306 doi:10.1029/2004GL022144
[7] Wenk H-R, Matthies S, Hemley R J, Mao H-K and Shu J 2000 *Nature* **405** 1044–7
[8] Merkel S, Wenk H-R, Shu J, Shen G, Gillet P, Mao H-K and Hemley R J 2002 *J. Geophys. Res.* **107** B11 2271 doi:10.1029/2001JB000920
[9] Ischia G, Wenk H-R, Lutterotti L and Berberich F 2005 *J. Appl. Crystallogr.* **38** 377–80
[10] Merkel S and Yagi T 2005 *Rev. Sci. Instrum.* **76** 046109
[11] Lutterotti L, Matthies S and Wenk H-R 1999 *Int. U. Crystallogr. Comm. Powder Diffraction Newsletter* **21** 14–5
[12] Hammersley A P 1998 *Internal Report* ESRF-98-HA01
[13] Finger L W and Hazen R M 1991 *Acta Crystallogr.* B **47** 561–80
[14] Matthies S, Priesmeyer H G and Daymond M R 2001 *J. Appl. Crystallogr.* **34** 585–601 doi:10.1107/S0021889801010482
[15] Shim S-H, Duffy T S and Shen G 2000 *Phys. Earth Planet. Inter.* **120** 327–38

[16] Shim S-H, Duffy T S and Shen G 2000 *J. Geophys. Res.* **105** 25955–68
[17] Popa N C and Balzar D 2001 *J. Appl. Crystallogr.* **34** 187–95 doi:10.1107/S0021889801002060
[18] Stout G H and Jensen L H 1989 *X-ray Structure Determination* (New York: Wiley–Interscience) p 189
[19] Young R A 1993 *The Rietveld Method* ed R A Young (New York: Oxford University Press) chapter 1, p 1
[20] Matthies S and Vinel G W 1982 *Phys. Status Solidi* b **112** K111–4
[21] Prince E 1993 *The Rietveld Method* ed R A Young (New York: Oxford University Press) chapter 3, p 43
[22] Merkel S 2006 *J. Phys.: Condens. Matter* **18** S949–62
[23] Singh A K 1993 *J. Appl. Phys.* **73** 4278–86
[24] Singh A K, Balasingh C, Mao H-K, Hemley R J and Shu J 1998 *J. Appl. Phys.* **83** 7567–75
[25] Shieh S R, Duffy T S and Shen G 2004 *Phys. Earth Planet. Inter.* **143/144** 93–105 doi:10.1016/j.pepi.2003.10.006
[26] Poirier J P, Beauchesne S and Guyot F 1989 *Perovskites, A.G.U. Monograph* vol 45, ed A Navrotsky and D Weidner (Washington, DC: Amer. Geophys. U.) pp 119–23
[27] Wang Z, Karato S-I and Fujino K 1993 *Phys. Earth Planet. Inter.* **79** 299–312
[28] Besson P, Poirier J P and Price G D 1996 *Phys. Chem. Minerals* **23** 337–44
[29] Karato S, Zhang S, Zimmerman M E, Daines M J and Kohlstedt D L 1998 *Pure Appl. Geophys.* **151** 589–603
[30] Skrotzki W and Haasen P 1981 *J. Physique Coll.* **42** C3 119
[31] Carter N L and Heard H C 1970 *Am. J. Sci.* **269** 193
[32] Wenk H-R, Canova G, Molinari A and Mecking H 1988 *Acta Metall.* **37** 2017–29
[33] Wenk H-R 2000 *Texture and Anisotropy. Preferred Orientations in Polycrystals and Their Effect on Materials Properties* 2nd paperback edn, ed U F Kocks, C N Tomé and H-R Wenk (Cambridge: Cambridge University Press) chapter 14, p 560